

# Global observations of large oceanic eddies

Dudley B. Chelton,<sup>1</sup> Michael G. Schlax,<sup>1</sup> Roger M. Samelson,<sup>1</sup> and Roland A. de Szoeke<sup>1</sup>

Received 26 May 2007; revised 13 June 2007; accepted 6 July 2007; published 9 August 2007.

[1] Ten years of sea-surface height (SSH) fields constructed from the merged TOPEX/Poseidon (T/P) and ERS-1/2 altimeter datasets are analyzed to investigate mesoscale variability in the global ocean. The higher resolution of the merged dataset reveals that more than 50% of the variability over much of the World Ocean is accounted for by eddies with amplitudes of 5–25 cm and diameters of 100–200 km. These eddies propagate nearly due west at approximately the phase speed of nondispersive baroclinic Rossby waves with preferences for slight poleward and equatorward deflection of cyclonic and anticyclonic eddies, respectively. The vast majority of the eddies are found to be nonlinear. **Citation:** Chelton, D. B., M. G. Schlax, R. M. Samelson, and R. A. de Szoeke (2007), Global observations of large oceanic eddies, *Geophys. Res. Lett.*, 34, L15606, doi:10.1029/2007GL030812.

## 1. Introduction

[2] The kinetic energy of mesoscale variability (scales of tens to hundreds of km and tens to hundreds of days) is more than an order of magnitude greater than the mean kinetic energy over most of the ocean [Wyrki *et al.*, 1976; Richardson, 1983]. Mesoscale variability occurs as linear Rossby waves and as nonlinear vortices or eddies. In contrast to linear waves, nonlinear vortices can transport momentum, heat, mass and the chemical constituents of seawater, and thereby contribute to the general circulation, large-scale water mass distributions, and ocean biology [Robinson, 1983].

[3] Distinguishing between Rossby waves and eddies is difficult because of the sampling requirements in both space and time. Our previous study based on T/P data alone [Chelton and Schlax, 1996] documented global westward propagation that was subsequently interpreted as linear baroclinic Rossby waves modified by various effects that are neglected in the classical theory [Killworth *et al.*, 1997; Dewar, 1998; de Szoeke and Chelton, 1999; Tailleux and McWilliams, 2001; LaCasce and Pedlosky, 2004; Killworth and Blundell, 2005]. However, some of the observed characteristics cannot be explained by existing theories, e.g., the propagation is westward with little meridional deflection [Challenor *et al.*, 2001] and with little evidence of the dispersion expected for Rossby waves [Chelton and Schlax, 2003]. The objective of this study is to investigate these characteristics from the higher

resolution SSH fields afforded by the merged T/P and ERS-1 and ERS-2 satellite datasets.

## 2. Data Processing

[4] SSH fields constructed by merging the data from T/P and the successive ERS-1 and ERS-2 altimeters [Ducret *et al.*, 2000] were obtained from Collecte Localis Satellites at 7-day intervals for the 10-year period October 1992–August 2002 with the 1993–1999 mean removed at each grid point. These residual SSH fields were zonally high-pass filtered to remove large-scale heating and cooling effects [Chelton and Schlax, 1996] and the resulting anomaly fields were smoothed with half-power filter cutoffs of  $3^\circ \times 3^\circ \times 20$  days to reduce mapping errors and improve the performance of the automated eddy tracking procedure (see Appendix A).

## 3. Eddy Characteristics

[5] The resolution of the merged T/P and ERS-1/2 data is about double that of the T/P data alone [Chelton and Schlax, 2003], which presents a markedly different picture of SSH (Figure 1). The merged data reveal many isolated eddy-like cyclonic and anticyclonic features (negative and positive SSH, respectively) that are poorly resolved in the T/P data alone. Animations of the data show that these eddies propagate considerable distances westward.

[6] Eddy trajectories were obtained by the automated tracking of a specific contour of the Okubo-Weiss parameter,  $W$ , selected for global analysis (see Appendix A). About 45% of the  $\sim 112,000$  tracked eddies poleward of  $10^\circ$  had tracking lifetimes  $\leq 3$  weeks. Globally, there is no preference for polarity; the numbers of long-lived cyclonic and anticyclonic eddies with lifetimes  $\geq 4$  weeks were 31,120 and 30,898, respectively (Figure 2). Regionally, however, there are some polarity preferences.

[7] Within the eddy-rich regions, more than 20 eddies with lifetimes  $\geq 4$  weeks were observed in each  $1^\circ$  bin over the 10-year data record (Figure 3a). There are vast areas in which eddies were seldom or never observed (e.g., the northeast Pacific and the midlatitude South Pacific). Eddies may exist in these regions, but with sizes too small to be resolved in the merged SSH fields because of noise in the data, the smoothing applied to the data, or the particular threshold value of the Okubo-Weiss parameter chosen here to define the eddies. The mean eddy amplitudes (Figure 3b) range from only a few cm in the low-energy regions to more than 20 cm near strong currents. Generally, both the eddy density and the mean eddy amplitude are largest in regions of large SSH standard deviation; few tracked eddies were detected in regions where the filtered SSH standard deviation is less than 4 cm. Notable exceptions are the eastern subtropical regions of the South Pacific and North Atlantic

<sup>1</sup>College of Oceanic and Atmospheric Sciences, Oregon State University, Corvallis, Oregon, USA.

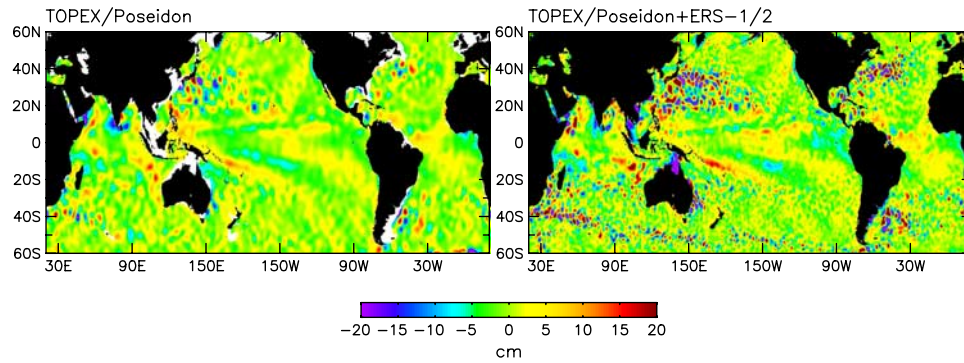


**Figure 1.** Representative maps of North Pacific SSH on 21 August 1996 from the T/P data alone and from the merged T/P and ERS-1/2 data.

where eddies are abundant but the SSH standard deviation is small.

[8] Except in the eastern North Pacific in association with the Central American wind jets, relatively few eddies are found at latitudes  $<20^\circ$ , possibly because most of the propagating energy in the tropics is in the form of Rossby waves rather than eddies. This is consistent with the presence of large-scale, curved crests and troughs of SSH that propagate westward in the tropical Pacific and Atlantic (Figure 1). Their curvature is characteristic of the  $\beta$ -refraction of Rossby waves caused by the poleward decrease in westward phase speed. They can be identified as far north as about  $50^\circ\text{N}$  in the far eastern North Pacific, but with westward penetration of

$<1000$  km at the high latitudes [Fu and Qiu, 2002]. They appear to be identifiable farther west at higher latitudes in the South Pacific.

[9] The mean eddy diameters as defined by the chosen  $W$  contour decrease from about 200 km in the eddy-rich low and middle latitude regions to about 100 km at high latitudes (Figure 3c). While the resolution limitations of the merged SSH dataset [Chelton and Schlax, 2003; Pascual et al., 2006] are undoubtedly a factor in the size distribution of the tracked eddies, this factor-of-2 decrease in diameters is very similar to the eddy scales noted previously from much higher-resolution along-track altimeter data [Stammer, 1997] and is small compared with the

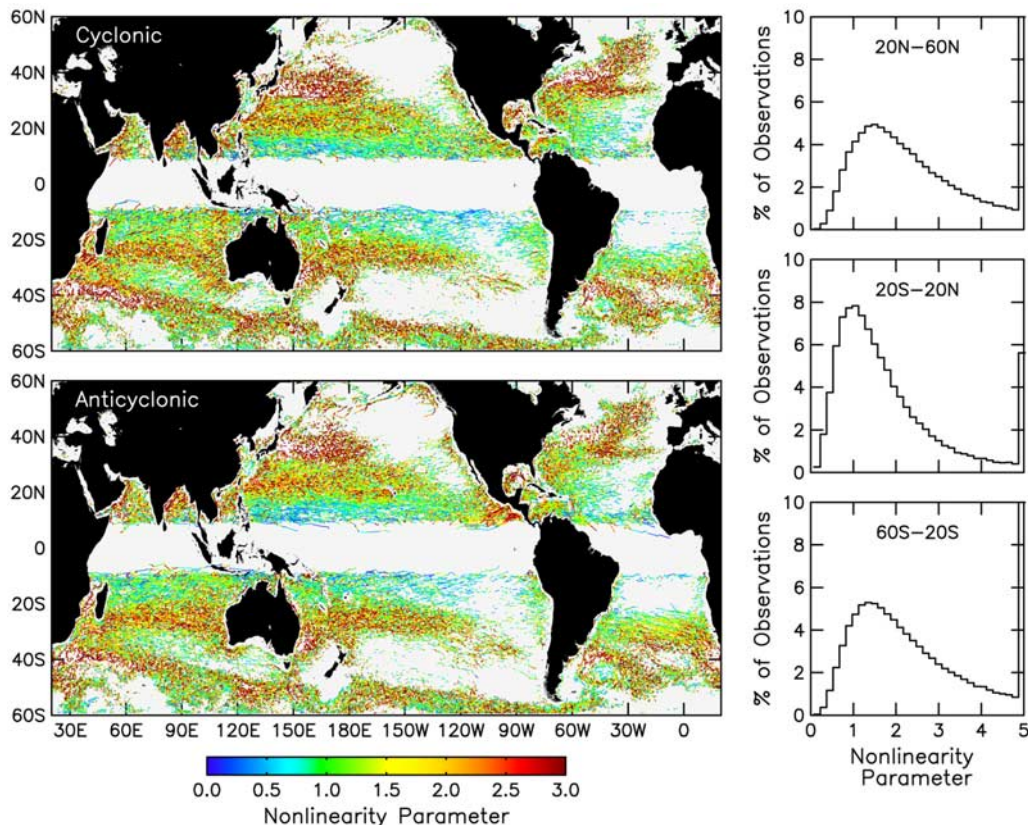


**Figure 2.** The trajectories of cyclonic and anticyclonic eddies with lifetimes  $\geq 4$  weeks that are located poleward of  $10^\circ$  of latitude at least once during their lifetime, with color coding of the nonlinearity parameter  $u/c$  (see text). (right) The distributions of  $u/c$  are shown for three latitude bands.

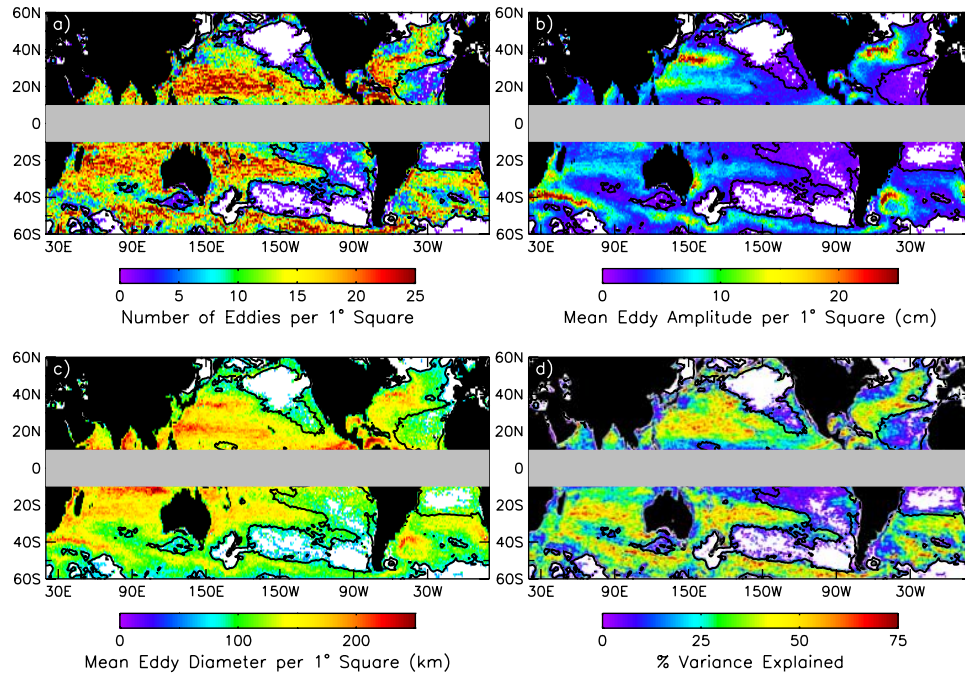


**Figure 3.** The eddy characteristics in  $1^\circ$  squares for eddies with lifetimes  $\geq 4$  weeks: (a) The number of eddies of both polarities (white areas correspond to no observed eddies); (b) the mean amplitude; (c) the mean diameter; and (d) the percentage of SSH variance explained (white areas correspond to 0%). The contour in each panel is the 4 cm standard deviation of filtered SSH.

order of magnitude latitudinal decrease in the Rossby radius that is often associated with eddy size. Such large eddy sizes relative to the Rossby radius have also been noted from in situ data in the subtropical North Pacific [Roemmich and Gilson, 2001].

[10] From altimetric estimates of spectral kinetic energy flux, it has been argued that there is evidence for an upscale nonlinear cascade of kinetic energy with an arrest scale similar to the large eddy diameters obtained here [Scott and

Wang, 2005]. Recent modeling supports this view and suggests that dissipation may play an important role in determining the large eddy diameters [Arbic and Flierl, 2004].

#### 4. Propagation Directions and Speeds

[11] A striking characteristic of the eddy trajectories is the strong tendency for purely westward propagation (Figure 4).

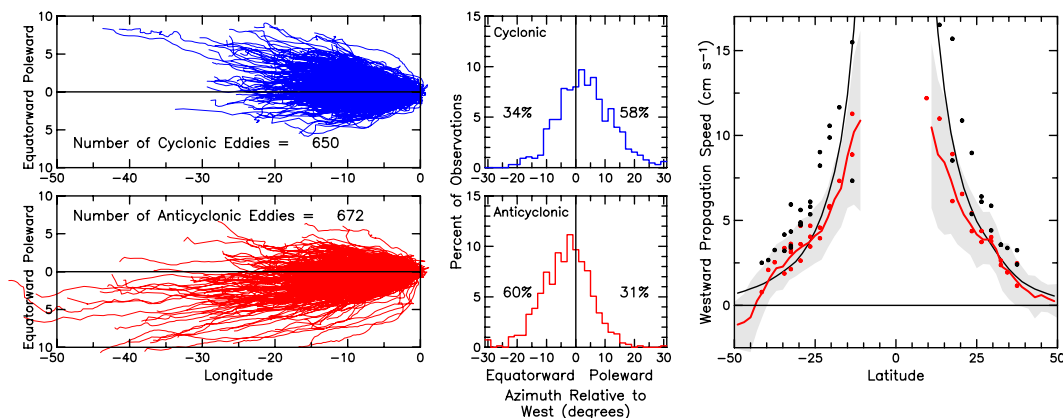


**Figure 4.** The global propagation characteristics of long-lived cyclonic and anticyclonic eddies with lifetimes  $\geq 12$  weeks. (left) The relative changes in longitude (negative westward) and latitude (poleward versus equatorward, both hemispheres combined). (middle) Histograms of the mean propagation angle relative to due west. (right) The latitudinal variation of the westward zonal propagation speeds of large-scale SSH (black dots) and small-scale eddies (red dots) along the selected zonal sections considered previously by Chelton and Schlax [1996]. The global zonal average of the propagation speeds of all of the eddies with lifetimes  $\geq 12$  weeks is shown in the right panel by the red line, with gray shading to indicate the central 68% of the distribution in each latitude band, and the propagation speed of nondispersive baroclinic Rossby waves is shown by the black line.



Only about  $\frac{1}{4}$  of the eddies had mean propagation directions that deviated by more than  $10^\circ$  from due west. Cyclonic and anticyclonic eddies have preferences for, respectively, small poleward and equatorward deflections (Figure 4 (middle)). Similar results have previously been obtained regionally [Morrow *et al.*, 2004]. Globally, the percentages of eddies that propagated with equatorward deflection, purely zonally ( $0^\circ \pm 1^\circ$ ), and with poleward deflection, respectively, were 34%, 8% and 58% for the cyclonic eddies and 60%, 9% and 31% for the anticyclonic eddies.

[12] Eddy propagation speeds were estimated from local least squares fits of the longitudes of eddy centroids as a function of time (Figure 4 (right)). Estimates did not depend significantly on eddy polarity. Equatorward of about  $25^\circ$ , eddy speeds are slower than the zonal phase speeds of nondispersive baroclinic Rossby waves predicted by the classical theory. In the Antarctic Circumpolar Current, nearly all of the eddies are advected eastward. Elsewhere, eddy speeds are very similar to the westward phase speeds of classical Rossby waves.

[13] The eddy propagation speeds deduced here differ from our previous analysis of large-scale SSH variability from the lower-resolution T/P dataset [Chelton and Schlax, 1996], which found that features poleward of about  $15^\circ$  propagate faster than the classical Rossby wave phase speed. The Radon transform analysis method of that study is insensitive to the smaller-scale eddies tracked here; when applied to the higher-resolution merged T/P and ERS-1/2 data along the same zonal sections, the Radon transform estimates of propagation speeds do not differ significantly from the speeds obtained from the T/P data alone (Figure 4). The apparent scale dependence of propagation speed suggests that SSH variability consists of a superposition of eddies and larger-scale, faster-propagating Rossby waves.

## 5. Nonlinearity

[14] The propagation speeds and directions of the observed extratropical eddies are consistent with theories for nonlinear vortices, which predict that eddies should propagate westward with little meridional deflection at the phase speeds of nondispersive baroclinic Rossby waves [McWilliams and Flierl, 1979; Cushman-Roisin, 1994]. The opposing weak meridional drifts of cyclonic and anticyclonic eddies are expected from the combination of the  $\beta$  effect and self advection. The widths of the distributions of meridional deflection angle in Figure 4 and the fact that nearly  $\frac{1}{3}$  of the observed eddies of each polarity had meridional deflections opposite of that expected may be consequences of eddy-eddy interactions and advection by background currents.

[15] The identification of many long-lived, coherent features with propagation characteristics predicted by nonlinear theories suggests that SSH variability outside of the tropics involves nonlinear dynamics. The degree of nonlinearity was conservatively estimated at each time step for every tracked eddy by computing the mean geostrophic speed within the closed  $W$  contour. The ratio of this particle speed  $u$  to the local translation speed  $c$  of the eddy provides a measure of nonlinearity; the dynamics are nonlinear when this ratio exceeds 1.

[16] Most of the observed nonlinearity ratios are between 1 and 4. Tracked features are less nonlinear in the tropics than in the extratropics (Figure 2 (right)). This is also evident from the maps of eddy trajectories; most of the linear mesoscale features are restricted to the latitude band between about  $20^\circ\text{S}$  and  $20^\circ\text{N}$  (Figure 2 (left)). Globally, 83% of the weekly observations for the long-lived eddies with lifetimes  $\geq 4$  weeks were nonlinear and 94% of the tracked eddies were nonlinear at least once during their lifetime.

## 6. Discussion

[17] The merged T/P and ERS-1/2 data reveal that much of the mesoscale variability outside of the tropics consists of nonlinear eddies. This contrasts with our earlier study based on lower-resolution SSH fields constructed from T/P data alone which concluded that SSH variability consists largely of linear Rossby waves modified by various effects that are neglected in the classical theory. In addition to explaining the nearly due west propagation of observed mesoscale variability, the nonlinearity and long lifetimes of the eddies explain the observed weak dispersion in wavenumber-frequency spectra of SSH [Chelton and Schlax, 2003]; because the eddies retain their shapes as they propagate, the energy at every wavenumber propagates at the same speed, i.e., nondispersively.

[18] Quantifying the percentage of SSH variance accounted for by eddies is subjective, in part because the “edge” of an eddy is not clearly defined. In the eddy-rich regions, the area within the chosen  $W$  contour accounts for more than 50% of the variance of the filtered SSH fields from consideration of only the eddies with lifetimes  $\geq 4$  weeks (Figure 3d). The remaining variance is attributable to eddies with shorter lifetimes, failures of the tracking algorithm, and physical processes other than eddies (e.g., Rossby waves). There is doubtless also SSH variability at space-time scales shorter than can be resolved in the merged SSH data.

[19] The observed eddies are likely generated by instabilities of the background currents [Gill *et al.*, 1974; Stammer, 1997; Arbic and Flierl, 2004; Scott and Wang, 2005] or by the instability of Rossby waves themselves [LaCasce and Pedlosky, 2004]. These eddies are important to ocean biology [Robinson, 1983] and likely facilitate significant heat transport such as has been observed in the subtropical North Pacific from in situ measurements of the vertical structures of the temperature and velocity fields associated with 410 eddies observed in the altimeter data [Roemmich and Gilson, 2001]. The widespread existence of relatively large and trackable eddies thus has direct implications for the role of the oceans in the global heat balance.

## Appendix A: Automated Eddy-Tracking Procedure

[20] Eddies were identified by closed contours of the Okubo-Weiss parameter,  $W$ , which is a measure of the relative importance of deformation and rotation and is given by the sum of the squares of the normal and shear components of strain minus the square of the relative vorticity [Isern-Fontanet *et al.*, 2003, 2006]. For the horizontally nondivergent flow in the ocean, this reduces to  $W = 4(u_x^2 +$

$v_x u_y$ ), where subscripts denote partial differentiation and the eastward and northward velocity components were computed geostrophically from the altimeter data by  $u = -(g/f)h_y$ , and  $v = (g/f)h_x$ , where  $h$  is the SSH,  $g$  is the gravitational acceleration and  $f$  is the Coriolis parameter.

[21] Eddies, in which vorticity dominates strain, are marked by negative  $W$ . For the global analysis presented here, closed contours of  $W = -2 \times 10^{-12} \text{ s}^{-2}$  were taken to define eddies. SSH, either wholly negative or wholly positive within such contours, indicates cyclonic or anticyclonic polarity, respectively. To avoid tracking noise-induced artifacts, each resulting  $W$  field was smoothed with half-power filter cutoffs of  $1.5^\circ \times 1.5^\circ$  and only cases for which the  $W$  contour enclosed at least four  $0.25^\circ$  pixels, equivalent to an area of about  $(50 \text{ km})^2$ , were considered. The center location of the eddy was defined to be the centroid of SSH within the  $W$  contour and the eddy diameter was defined to be that of a circle with area equal to that enclosed by the  $W$  contour. Numerical errors incurred in the squared double differentiation of  $h$  to obtain  $W$  are amplified by the factor  $f^{-2}$ . Since  $f$  tends to zero at the equator, attention was restricted to eddies centered outside of  $10^\circ\text{S}$   $10^\circ\text{N}$  at least once during their lifetime.

[22] Automated tracking of eddies was based on a modified version of a procedure developed previously [Isern-Fontanet et al., 2003, 2006]. Each eddy was tracked from one 7-day time step to the next by finding the closest eddy center in the later map. To avoid jumping from one track to another, the search area in the later map was restricted to the interior of an ellipse with zonally oriented major axis, eastern focus at the current eddy, and a minor axis of  $2^\circ$  of latitude. The distance from the eastern focus to the eastern extremum of the ellipse was  $1^\circ$  of longitude. In concert with the observed decrease of propagation speeds with increasing latitude, the longitudinal distance from the eastern focus to the western extremum of the ellipse decreased from  $10^\circ$  at low latitudes to  $1^\circ$  at latitudes higher than  $20^\circ$ . If a single eddy was closest to more than one eddy in the earlier map, it was assigned to the eddy with the longest track up to that point.

[23] The above parameters of the automated tracking procedure were selected for the global analysis presented here. While the results are not strongly sensitive to the details, the tracking can be improved somewhat regionally by fine tuning the tracking parameters [Isern-Fontanet et al., 2003, 2006; Morrow et al., 2004]. For example, smaller values of  $W$  result in more tracked eddies in regions of small SSH variance but reduce the number of tracked eddies in regions of large SSH variance. Larger values of  $W$  have the opposite effect.

[24] **Acknowledgments.** The merged altimeter dataset analyzed here was obtained from Collecte Localis Satellites in Toulouse, France. We thank D. Alsdorf, B. Arbic, J. Blundell, I. Cerovečki, P. Cipollini, W. Crawford, L.-L. Fu, P. Killworth, N. Maximenko, R. Matano, J. McWilliams, P. Niiler, L. Pratt, B. Qiu, P. Rhines, R. Scott, S. Smith, R. Tailleux and J. Theiss for helpful comments. This research was supported by contract 1206715 from the Jet Propulsion Laboratory funded as part of the NASA Ocean Surface Topography Mission and by NASA grant NNG05GN98G, ONR contract N00014-05-1-0891, and NSF grants OCE-0424516 and OCE-0220471.

## References

- Arbic, B. K., and G. R. Flierl (2004), Baroclinically unstable geostrophic turbulence in the limits of strong and weak bottom Ekman friction: Application to midocean eddies, *J. Phys. Oceanogr.*, **34**, 2257–2273.
- Challenor, P. G., P. Cipollini, and D. Cromwell (2001), Use of the 3D Radon transform to examine the properties of oceanic Rossby waves, *J. Atmos. Oceanic Technol.*, **18**, 1558–1566.
- Chelton, D. B., and M. G. Schlax (1996), Global observations of oceanic Rossby waves, *Science*, **272**, 234–238.
- Chelton, D. B., and M. G. Schlax (2003), The accuracies of smoothed sea surface height fields constructed from tandem altimeter datasets, *J. Atmos. Oceanic Technol.*, **20**, 1276–1302.
- Cushman-Roisin, B. (1994), *Introduction to Geophysical Fluid Dynamics*, 320 pp., Prentice Hall, Upper Saddle River, N. J.
- de Szoeke, R. A., and D. B. Chelton (1999), The modification of long planetary waves by homogeneous potential vorticity layers, *J. Phys. Oceanogr.*, **29**, 500–511.
- Dewar, W. K. (1998), On “too fast” baroclinic planetary waves in the general circulation, *J. Phys. Oceanogr.*, **28**, 1739–1758.
- Ducet, N., P.-Y. Le Traon, and G. Reverdin (2000), Global high resolution mapping of ocean circulation from TOPEX/Poseidon and ERS-1/2, *J. Geophys. Res.*, **105**, 19,477–19,498.
- Fu, L.-L., and B. Qiu (2002), Low-frequency variability of the North Pacific Ocean: The roles of boundary- and wind-driven baroclinic Rossby waves, *J. Geophys. Res.*, **107**(C12), 3220, doi:10.1029/2001JC001131.
- Gill, A. E., J. S. A. Green, and A. J. Simmons (1974), Energy partition in the large-scale ocean circulation and the production of mid-ocean eddies, *Deep Sea Res.*, **21**, 499–528.
- Isern-Fontanet, J., E. Garcia-Ladona, and J. Font (2003), Identification of marine eddies from altimetric maps, *J. Atmos. Oceanic Technol.*, **20**, 772–778.
- Isern-Fontanet, J., E. Garcia-Ladona, and J. Font (2006), Vortices of the Mediterranean Sea: An altimetric perspective, *J. Phys. Oceanogr.*, **36**, 87–103.
- Killworth, P. D., and J. R. Blundell (2005), The dispersion relation for planetary waves in the presence of mean flow and topography. Part II: Two-dimensional examples and global results, *J. Phys. Oceanogr.*, **35**, 2110–2133.
- Killworth, P. D., D. B. Chelton, and R. A. de Szoeke (1997), The speed of observed and theoretical long extra-tropical planetary waves, *J. Phys. Oceanogr.*, **27**, 1946–1966.
- LaCasce, J. H., and J. Pedlosky (2004), The instability of Rossby basin modes and the oceanic eddy field, *J. Phys. Oceanogr.*, **34**, 2027–2041.
- McWilliams, J. C., and G. R. Flierl (1979), On the evolution of isolated, nonlinear vortices, *J. Phys. Oceanogr.*, **9**, 1155–1182.
- Morrow, R., F. Birol, D. Griffin, and J. Sudre (2004), Divergent pathways of cyclonic and anti-cyclonic ocean eddies, *Geophys. Res. Lett.*, **31**, L24311, doi:10.1029/2004GL020974.
- Pascual, A., Y. Faugere, G. Larnicol, and P.-Y. Le Traon (2006), Improved description of the ocean mesoscale variability by combining four satellite altimeters, *Geophys. Res. Lett.*, **33**, L02611, doi:10.1029/2005GL024633.
- Richardson, P. L. (1983), Eddy kinetic energy in the North Atlantic Ocean from surface drifters, *J. Geophys. Res.*, **88**, 4355–4367.
- Robinson, A. R. (Ed.) (1983), *Eddies in Marine Science*, 609 pp., Springer, New York.
- Roemmich, D., and J. Gilson (2001), Eddy transport of heat and thermocline waters in the North Pacific: A key to interannual/decadal climate variability?, *J. Phys. Oceanogr.*, **31**, 675–687.
- Scott, R. B., and F. Wang (2005), Direct evidence of an oceanic inverse kinetic energy cascade from satellite altimetry, *J. Phys. Oceanogr.*, **35**, 1650–1666.
- Stammer, D. (1997), Global characteristics of ocean variability estimated from regional TOPEX/Poseidon altimeter measurements, *J. Phys. Oceanogr.*, **27**, 1743–1769.
- Tailleux, R., and J. C. McWilliams (2001), The effect of bottom pressure decoupling on the speed of extratropical, baroclinic Rossby waves, *J. Phys. Oceanogr.*, **31**, 1461–1476.
- Wyrki, K., L. Magaard, and J. Hager (1976), Eddy energy in the oceans, *J. Geophys. Res.*, **81**, 2641–2646.

D. B. Chelton, R. A. de Szoeke, R. M. Samelson, and M. G. Schlax, College of Oceanic and Atmospheric Sciences, Oregon State University, Corvallis, OR 97331-5503, USA. (chelton@coas.oregonstate.edu)